International Journal of Solids and Structures 102–103 (2016) 10–20

Contents lists available at ScienceDirect

International Journal of Solids and Structures

journal homepage: www.elsevier.com/locate/ijsolstr

A unified solution approach for a large variety of antiplane shear and torsion notch problems: Theory and examples

Marco Salviato[a,*], Michele Zappalorto[b]

[a] William E. Boeing Department of Aeronautics & Astronautics, University of Washington, 311D Guggenheim Hall, Seattle, WA 98195-2400, USA
[b] University of Padova, Department of Management and Engineering, Stradella San Nicola 3 – 36100 Vicenza Italy

ARTICLE INFO

Article history:
Received 7 April 2016
Revised 8 September 2016
Available online 27 October 2016

Keywords:
Antiplane shear
Torsion
Notch
Stress distributions

ABSTRACT

In this work, a unified solution approach is proposed for the analytical evaluation of the stress fields close to notches under antiplane shear and torsion loadings, which allows a large variety of notch problems to be tackled. The method is based on the complex potential approach for antiplane elasticity combined with the use of proper conformal mappings. In particular, it is shown that a well defined analytical link does exist between the complex potential to be used to determine stresses and the first derivative of the conformal mapping used to mathematically describe the notch profile. This makes some methodologies such as Schwarz-Christoffel transformation, which allows describing any polygonal domain automatically, very attractive for the direct solution of notch problems. A bulk of solutions are provided to support this finding, from cracks and pointed notches, to radiused notches. In addition, the accuracy of each proposed solution is discussed in detail taking advantage of a bulk of results from FE analyses.

1. Introduction

The knowledge of the linear elastic stress fields ahead of geometrical variations, such as notches, holes and cutouts, is essential in the design of mechanical components, where such variations are unavoidable.

Due to its simplicity in terms of constitutive equations, especially when compared to the plane stress or plane strain approximations, the mechanical model of longitudinal (antiplane) shear has received a special attention since the early investigations of stress fields around grooves or cracks, as documented by the oldated papers by Filon (1900); Shepherd (1932) Wigglesworth and Stevenson (1939) and Wigglesworth (1939) or by the extensive analysis carried out by Neuber (1958 and 1985) on circumferentially shafts under torsion with '*deep*' and '*shallow*' notches.

Some years later, Creager and Paris (1967) gave the elastic stress fields in the vicinity of the tip of isotropic blunt cracks, or '*slim*' parabolic notches, under Mode I, II and III loadings, where the extension of such a solution to anisotropic materials is more recent (Zappalorto and Carraro, 2015).

Due to the progress of advanced computational technology, far less attention was paid to analytical tools, and various numerical techniques were used to obtain the stress concentration factor of notched components subjected to torsion or antiplane shear (see, amongst others, Rushton, 1967; Hamada and Kitagawa, 1968; Matthews and Hooke, 1971, and Peterson, 1974; Noda and Takase, 2006; Zappalorto et al., 2011).

Motivated by the fact that the engineering use of torque carrying shafts is extensive and they are susceptible to crack formation at notches and grooves, in the recent years Zappalorto and co-workers carried out an extensive analysis on the stress fields close to notches in shafts under torsion, including semi-elliptical notches (Lazzarin et al., 2007), parabolic and hyperbolic notches (Zappalorto et al., 2008), U and V-shaped rounded notches (Zappalorto et al., 2010), V notches with end holes (Zappalorto and Lazzarin 2011a), inclined notches and shouldered fillets (Zappalorto and Lazzarin, 2011b) and notched tubes (Zappalorto and Lazzarin, 2012). In all these works, the stress field is obtained in closed form by taking advantage of the complex potential approach for antiplane elasticity, and using appropriate ad hoc complex functions for each case. It is also worth of mention that Zappalorto et al. showed that previously published solutions related to mode III loadings (Creager and Paris, 1967; Kullmer, 1992; Seweryn and Molski, 1996; Dunn et al., 1997; Qian and Hasebe, 1997), could be seen as special cases of their more general solutions.

Using the method of singular integral equations, the distribution of stresses over the contour of a rounded V-shaped notch under antiplane deformation was also investigated by Savruk et al. (2012), who later moved their attention also to quasi-orthotropic materials (Kazberuk et al., 2016), whereas the problem of stress

* Corresponding author.
E-mail addresses: salviato@aa.washington.edu (M. Salviato), michele.zappalorto@unipd.it (M. Zappalorto).

http://dx.doi.org/10.1016/j.ijsolstr.2016.10.022
0020-7683/

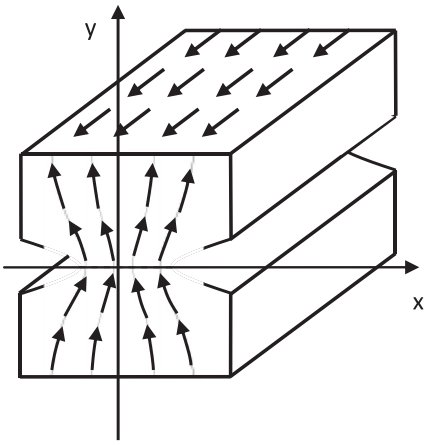

Fig. 1. Notched body under longitudinal shear.

singularity of a V-notch with angularly inhomogeneous elastic properties was recently addressed by Cheng et al. (2016).

The problem of the analytical evaluation of the stress fields close to notches under antiplane shear and torsion loadings is reconsidered in this work, where a universal solution approach is proposed which allows a large variety of notch problems to be tackled. The method is based on the complex potential approach for antiplane elasticity combined with conformal mapping. It is shown that a well defined analytical link does exist between the complex potential to be used to determine stresses and the first derivative of the conformal mapping used to mathematically describe the notch profile. This makes some methodologies such as Schwarz-Christoffel transformation, which allows describing any polygonal domain automatically, very attractive for the direct solution of notch problems. A bulk of solutions are provided to support this finding, from cracks and pointed notches, to radiused notches. In addition, the accuracy of each proposed solution is discussed in detail taking advantage of a number of results from FE analyses.

2. Preliminary remarks

Consider a body made of a homogenous and isotropic material obeying the theory of the linear elastic deformations. Further, consider the Cartesian reference system (x,y,z) represented in Fig. 1 and suppose that the body is loaded by a remote shear stress τ_∞ resulting only in displacements w in the z direction, normal to the plane of the notch characterized by the x and y axes (Fig. 1).

Coupling equilibrium of stresses and compatibility of strains results in the following two-dimensional Laplace equation to be integrated (Timoshenko and Goodier, 1970):

$$\frac{\partial^2 w}{\partial x^2}+\frac{\partial^2 w}{\partial y^2}=0 \tag{1}$$

so that the displacement component w is a harmonic function. The solution of Eq. (1) in a given two-dimensional domain $\Omega\cup\partial\Omega$ (where $\partial\Omega$ = domain boundary, Ω = inner portion of the domain), requires that the function $w\in C^2(\Omega)$ and satisfies prescribed boundary conditions. It is worth mentioning that, in the present work, the use of Eq. (1) is restricted to simply connected domains only.

An important issue to be addressed in solving for w is the shape of the domain $\Omega\cup\partial\Omega$. Indeed, standard methods of solution, such as separation of variables, can be employed only for simple enough shapes, i.e. rectangular or circular. This gives rise to the interest in finding a suitable change of variables transforming $\Omega\cup\partial\Omega$ into a simpler domain $\Omega'\cup\partial\Omega'$, easier to be addressed. Of course, such a transformation, $\{u=u(x, y), v=v(x, y)\}$, is required to be bijective in order to avoid any ambiguity in moving from a domain to the other.

In case the choice of u and v is restricted to functions being C^2 in Ω and satisfying the following equations:

$$\frac{\partial u}{\partial x}=\frac{\partial v}{\partial y}\qquad \frac{\partial u}{\partial y}=-\frac{\partial v}{\partial x}\qquad \text{in }\Omega \tag{2a,b}$$

i.e being the real and imaginary parts of an analytic function $f(z)$ respectively, Eq. (1) can be recast again as a Laplace equation in the transformed domain Ω' (Savin 1970; Greenberg 2001):

$$\frac{\partial^2\omega}{\partial u^2}+\frac{\partial^2\omega}{\partial v^2}=0 \tag{2c}$$

where now $\omega(u, v)=w\{x(u, v), y(u, v)\}$. The integration domain can be made simpler without affecting the simplicity of the governing equation on condition that a conformal transformation of variables is considered. In other words, if the transformation of coordinates can be expressed by a complex analytic function, so that $u(x,y)$ and $v(x,y)$ are conjugate harmonics, the Laplace equation is preserved and the shape of the domain can be made sufficiently simple to perform integration by separation of variables methods. The interested reader can find a comprehensive review on this subject in the book by Greenberg (Greenberg 2001), among others.

3. Analytical framework to the notch stress assessment

3.1. Notch described by the condition $u(x, y)=u_0$

Let us consider a notch profile and a conformal map $z=z(\xi)$ with $\xi=u+iv$ and $z=x+iy$ such that the notch profile is described by the condition $u(x, y)=u_0$. The constant u_0 is taken as a positive number, so that the domain of integration belong to the right half plane of the (u,v) space. Under this condition, u is always positive whilst v can take any value.

Thus, Eq. (2c) can be solved assuming separation of variables in curvilinear coordinates:

$$\omega=f(u)g(v) \tag{3}$$

Substituting Eq. (3) into (2c) leads to:

$$f''(u)g(v)+f(u)g''(v)=0 \tag{4}$$

or, equivalently:

$$\frac{f''(u)}{f(u)}=-\frac{g''(v)}{g(v)}=\lambda^2 \tag{5}$$

where λ is real a constant. Accordingly, the governing PDE can be simplified into two ODE in the variables u, v:

$$f''(u)-\lambda^2 f(u)=0\qquad g''(v)+\lambda^2 g(v)=0 \tag{6}$$

With the aim to introduce the relevant boundary conditions, the following expressions for strains and stresses in curvilinear coordinate are useful (Sokolnikoff, 1983):

$$\gamma_{iz}=\frac{1}{h_i}\frac{\partial\omega}{\partial\alpha_i}\qquad \tau_{iz}=\frac{G}{h_i}\frac{\partial\omega}{\partial\alpha_i} \tag{7}$$

where G is the elastic modulus in shear and h_i is the factor of distortion (Neuber, 1958).

Since, in general $h_i\neq 0$, the *Dirichlet conditions* in terms of stresses result in *Von Neuman* conditions on ω.

The problem is then defined by the following system of equations:

$$\begin{cases} g''(v) + \lambda^2 g(v) = 0 \\ f''(u) - \lambda^2 f(u) = 0 \\ f'(u_0) = 0 \\ \frac{|f'(u)|}{h_u} < \infty \quad \text{for} \quad u, v \to \infty \\ \frac{|g'(v)|}{h_v} < \infty \quad \text{for} \quad u, v \to \infty \end{cases} \tag{8a,e}$$

where Eq. (8c) is the free-of-stress condition along the notch edge, whereas Eqs. (8d,e) express the condition for bounded stresses far away the notch tip.

The case $\lambda^2 \neq 0$ can be disregarded since it provides trivial solutions only. Differently, under the condition $\lambda^2 = 0$, the general solution:

$$\omega(u, v) = (A + Bu)(C + Dv) \tag{9}$$

can be further simplified into Eq. (10) to account for boundary conditions:

$$\omega(u, v) = C_1 + C_2 v \tag{10}$$

where C_1 represents a rigid translation which does not contribute to the strain field and can be ignored.

Introducing Eq. (10) into the definition of stresses and invoking Cauchy-Riemann conditions, one gets the following expressions:

$$\tau_{zx} = \varsigma \frac{\partial v}{\partial x} \qquad \tau_{zy} = \varsigma \frac{\partial u}{\partial x} \tag{11}$$

$\varsigma = GC_2$ being a constant to determine. It is worth noting that, since $\xi' = d\,\xi(z)/dz = \partial u/\partial x + i\partial v/\partial x$, shear stresses represent the real and imaginary parts of the first derivative of the conformal map used to describe the notch profile, $\xi = \xi\ (z)$:

$$\tau_{zy} + i\tau_{zx} = \varsigma \frac{d\xi(z)}{dz} \tag{12}$$

This result provides an explicit link between the domain geometry and the stress field. Once a suitable conformal map is found, the problem of finding the generated stress field can be solved directly, except for one constant ς, which can be found analytically for finite notches and cracks or it can be generally computed by FE analysis.

3.2. Notch described by the condition v(x, y) = v_0

Sometimes it is convenient to describe the notch profile by the condition $v(x, y) = v_0$. This is the case, for instance, in which the conformal map used to describe the domain is constructed by the *Schwarz-Christoffel* transformation.

The derivation of the stress field is similar to that provided in the foregoing section, provided that the following system of ODE is considered:

$$\begin{cases} g''(v) - \lambda^2 g(v) = 0 \\ f''(u) + \lambda^2 f(u) = 0 \\ g'(v_0) = 0 \\ \frac{|g'(v)|}{h_v} < \infty \quad \text{for} \quad u, v \to \infty \\ \frac{|f'(u)|}{h_u} < \infty \quad \text{for} \quad u, v \to \infty \end{cases} \tag{13a,e}$$

which results in:

$$\tau_{zx} = \varsigma \frac{\partial u}{\partial x} \qquad \tau_{zy} = -\varsigma \frac{\partial v}{\partial x} \tag{14a,b}$$

or equivalently:

$$\tau_{zx} - i\tau_{zy} = \varsigma \frac{d\xi(z)}{dz} \tag{15}$$

ς being a constant to determine.

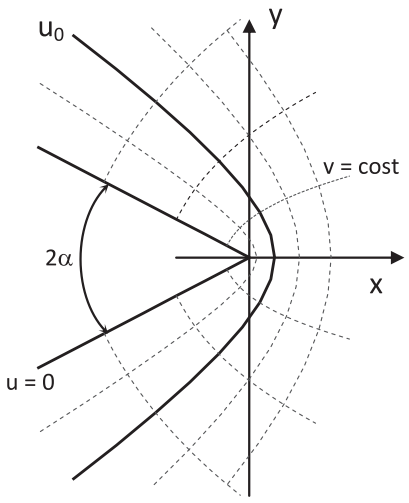

Fig. 2. Plot of conformal mapping given by Eq. (16).

4. Examples of applications to rounded notches

In this section several examples of application of the method proposed in the previous sections are presented. Initially, in order to prove the efficacy of the approach, a number of solutions already published in the literature are derived, whilst, subsequently, efforts are devoted to determine several new solutions for solids under antiplane shear and torsion and weakened by sharp and radiused notches.

4.1. Stresses on a body with a deep notch and a very large net ligament

Consider the mapping shown in Fig. 2 (Neuber, 1958 and 1985):

$$z = \xi^q \tag{16}$$

where $z = x + iy$ and $\xi = u_0 + iv$ and parameter q is linked to the notch opening angle by the expression $q = \frac{2\pi - 2\alpha}{\pi}$. The case $u_0 = 0$ represents the pointed V-notch case. More generally, such a mapping allows one to describe parabolic ($q = 2$) and hyperbolic ($1 < q < 2$) notch profiles in an infinite body. Substituting Eq. (16) into (12) results in:

$$\tau_{zy} + i\tau_{zx} = \varsigma \frac{d\xi(z)}{dz} = Az^{1/q-1} \tag{17}$$

where A is a real constant to determine. Accordingly, shear stress components are:

$$\begin{aligned} \tau_{zy} &= Ar^{1/q-1} \cos[(1/q - 1)\vartheta] \\ \tau_{zx} &= Ar^{1/q-1} \sin[(1/q - 1)\vartheta] \end{aligned} \tag{18}$$

in agreement with Zappalorto et al. (2008).

By a practical point of view, the solution can be successfully applied either to deep notches in infinite members or to deep notches in finite size components. In the latter case, whenever the notch depth is much larger than the member width, stresses can be fully computed analytically (see Zappalorto et al., 2008).

However, in the most general case, parameter A can be expressed as a function of the maximum notch tip stress:

$$A = \tau_{max} r_0^{1-1/q} \tag{19}$$

where $r_0 = u_0^q = \frac{q-1}{q} \cdot \rho$, ρ being the curvature radius at the notch tip (Neuber, 1958).

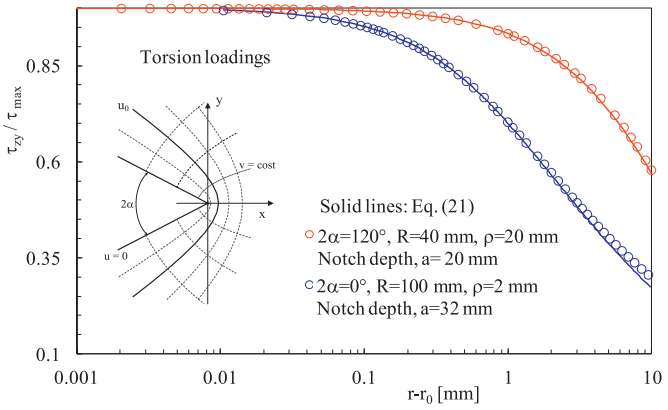

Fig. 3. Plot of the stress component along the notch bisector line. The stress component is normalised with respect to the maximum shear stress. Circumferential hyperbolic and parabolic notches in axis-symmetric shafts under torsion.

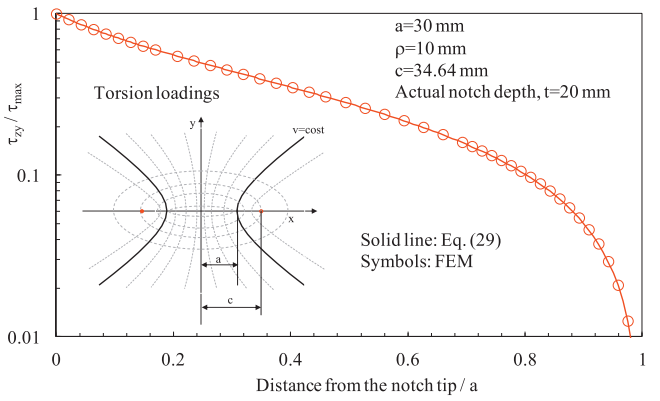

Fig. 5. Plot of the stress component along the notch bisector line. The stress component is normalised with respect to the maximum shear stress. Circumferential hyperbolic notch in an axis-symmetric shaft under torsion.

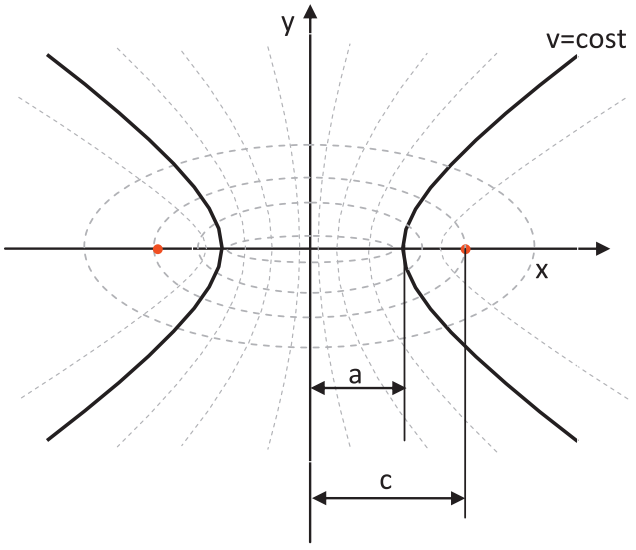

Fig. 4. Plot of conformal mapping given by Eq. (22).

Along the bisector line, the stress field close to the notch tip is:

$$\tau_{zy} = \tau_{max}\left(\frac{r_0}{r}\right)^{1-1/q} \tag{20}$$

Eq. (20) can be approximately extended to the case of an axis-symmetric notched shaft, with a net section of radius R, under torsion loadings by taking into account the linear decrease of the nominal shear stress:

$$\tau_{zy} = \tau_{max}\left(\frac{r_0}{r}\right)^{1-1/q} \times \left(1 - \frac{r - r_0}{R}\right) \tag{21}$$

A comparison between the analytical solution given by Eq. (21) and the results from some FE analyses carried out on axis-symmetric notched shafts under torsion is shown in Fig. 3, where a very satisfactory agreement can be noted.

4.2. Stresses on a body with a deep notch and a finite net ligament

Consider the mapping shown in Fig. 4 (Timoshenko and Goodier, 1970):

$$z = c \cdot \cosh\xi \tag{22}$$

where $z = x + iy$ and $\xi = u + iv_0$ and c is a constant. The case $v_0 = 0$ represents the deep crack case whereas, more generally, such a mapping allows a hyperbolic notch with foci at $x = \pm c$ to be described. Eq. (22) can be re-written as:

$$\xi = \operatorname{Arccosh}\frac{z}{c} \tag{23}$$

Substituting Eq. (23) into Eq. (15) results in:

$$\tau_{zx} - i\tau_{zy} = \varsigma\frac{d\xi(z)}{dz} = \frac{A}{\sqrt{z^2 - c^2}} = \frac{A}{c}\frac{1}{\sinh\xi} \tag{24}$$

where *A* is a real constant to determine. Since:

$$\frac{1}{\sinh\xi} = \frac{2\cos v \sinh u - 2i\sin v \cosh u}{\cosh 2u - \cos 2v} \tag{25}$$

stresses turn out to be:

$$\tau_{zx} = \frac{A_1 \cos v \sinh u}{\cosh 2u - \cos 2v} \qquad \tau_{zy} = \frac{A_1 \sin v \cosh u}{\cosh 2u - \cos 2v} \tag{26}$$

in agreement with Zappalorto et al. (2008). Parameter A_1 can be written as a function of the maximum notch tip stress:

$$A_1 = \tau_{max}\frac{1 - \cos 2v_0}{\sin v_0} = \frac{2\tau_{max}}{\sqrt{1 + \frac{a}{\rho}}} \tag{27}$$

Along the notch bisector line the stress field is:

$$\tau_{zy} = \frac{\tau_{max}}{\sqrt{1 + \frac{a}{\rho}}} \times \frac{1}{\sqrt{1 - \left(\frac{x}{c}\right)^2}} \tag{28}$$

As done in the previous section, Eq. (28) can be approximately extended the case of an axis-symmetric notched shaft under torsion loadings:

$$\tau_{zy} = \frac{\tau_{max}}{\sqrt{1 + \frac{a}{\rho}}} \times \frac{1}{\sqrt{1 - \left(\frac{x}{c}\right)^2}} \times \frac{x}{a} \tag{29}$$

where a is the radius of the net section and ρ is the notch root radius.

A comparison between the analytical solution given by Eq. (29) and the results from a FE analysis carried out on an axis-symmetric notched shaft under torsion is shown in Fig. 5, where a very satisfactory agreement can be noted.

4.3. Stresses on a body with a shallow notch and a very large net ligament

Consider the mapping shown in Fig. 6:

$$z = (1 - k)\,\xi + k\sqrt{\xi^2 + 4a^2} \tag{30}$$

where $z = x + iy$, $\xi = u_0 + iv$, and k and a are two constants.

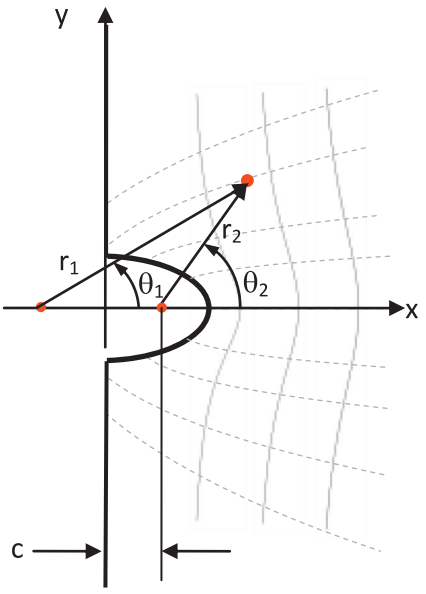

Fig. 6. Plot of conformal mapping given by Eq. (30).

Substituting $u_0 = 0$ allows a semi-elliptical notch to be obtained with depth, root radius and foci equal to:

$$t = k \cdot 2a \qquad \rho = 2a \cdot \frac{(1-k)^2}{k} \qquad c = 2a\sqrt{2k-1} \tag{31}$$

respectively. The case k tending to 1 represents the sharp crack case of length 2a, whereas for k tending to 0.5 a semicircular notch can be obtained. Eq. (30) can also be re-written as:

$$\xi = \frac{z(k-1) + k \cdot \sqrt{z^2 - 4a^2(2k-1)}}{2k-1} \tag{32}$$

Substituting Eq. (32) into (12) results in:

$$\tau_{zy} + i\tau_{zx} = A\left[\frac{k-1}{2k-1} + \frac{kz}{2k-1} \cdot \frac{1}{\sqrt{z^2 - c^2}}\right] \tag{33}$$

where A is a real constant to determine. Considering the two Cartesian reference systems centred on the ellipse foci, ($x_1 = x - c$, y) and ($x_2 = x + c$, y), Eq. (33) can be re-written as (see also Fig. 6):

$$\tau_{zx} = A\frac{k}{2k-1}\frac{r}{\sqrt{r_1 r_2}}\sin\left(\theta - \frac{\theta_1+\theta_2}{2}\right)$$
$$\tau_{zy} = A\frac{k}{2k-1}\left\{\frac{k-1}{k} + \frac{r}{\sqrt{r_1 r_2}}\cos\left(\theta - \frac{\theta_1+\theta_2}{2}\right)\right\} \tag{34}$$

where:

$$r_k = \sqrt{x_k^2 + y^2} \qquad \theta_i = \mathrm{Arg}[x_k + iy] \qquad (k = 1, 2) \tag{35}$$

Parameter A can be determined as a function of the far applied shear stress imposing $\tau_{zy} + i\tau_{zx} = \tau_\infty$ for $z \to \infty$. This condition, in view of Eq. (33), yields $A = \tau_\infty$. Along the notch bisector line the stress field simplifies as:

$$\tau_{zy} = \frac{k}{2k-1}\tau_\infty\left\{\frac{k-1}{k} + \frac{x}{\sqrt{x^2 - c^2}}\right\} \tag{36}$$

for antiplane shear loadings and:

$$\tau_{zy} = \frac{k}{2k-1}\tau_\infty\left\{\frac{k-1}{k} + \frac{x}{\sqrt{x^2 - c^2}}\right\} \times \left(1 - \frac{x-t}{R}\right) \tag{37}$$

in the case of a shallow notch in a finite size axis-symmetric shaft under torsion loadings of which the radius of the net section is R

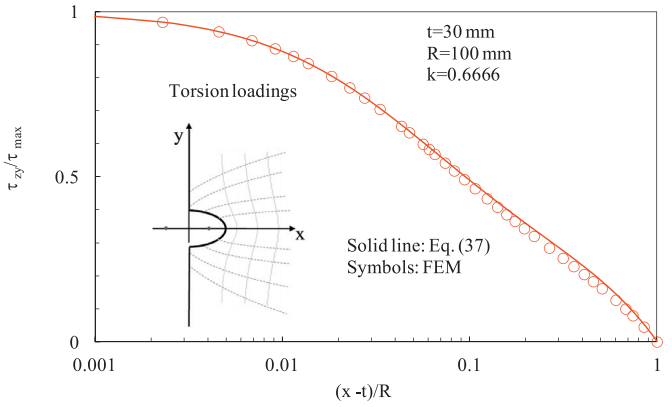

Fig. 7. Plot of the stress component along the notch bisector line. The stress component is normalised with respect to the maximum shear stress. Circumferential semi-elliptical notch in an axis-symmetric shaft under torsion.

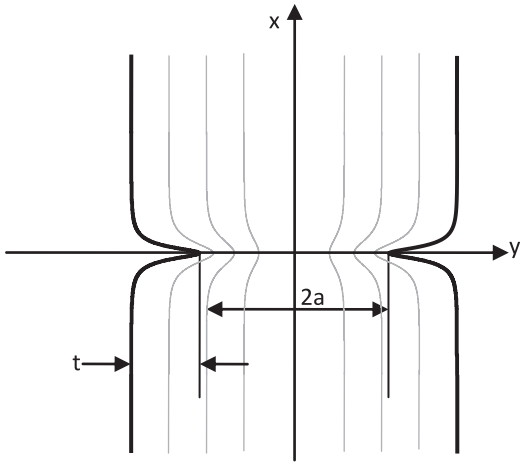

Fig. 8. Plot of conformal mapping given by Eq. (39).

(with a<<R). At the notch tip (x = t) one obtains:

$$\tau_{max} = \tau_\infty\left(1 + \frac{k}{1-k}\right) = \tau_\infty\left(1 + \sqrt{\frac{t}{\rho}}\right) \tag{38}$$

according to Neuber (1958).

A comparison between the analytical solution given by Eq. (37) and the results from a FE analysis carried out on an axis-symmetric notched shaft under torsion is shown in Fig. 7, where a very satisfactory agreement can be noted.

4.4. Stresses on a body with a finite notch and a finite net ligament

Consider the mapping shown in Fig. 8:

$$z = k_1 \cdot \mathrm{Arcsinh}\left\{\frac{\sinh\xi}{k_2}\right\} \tag{39}$$

where $z = x + iy$, $\xi = u + iv_0$, and k_1 and k_2 are two constants. Such a mapping allows the case of a finite depth notch in a finite size solid to be treated letting $v = v_0$. The resulting notch depth and net ligament of the specimen are:

$$t = k_1\left\{v_0 - \mathrm{Arcsin}\left(\frac{\sin v_0}{k_2}\right)\right\} \qquad a = k_1\mathrm{Arcsin}\left(\frac{\sin v_0}{k_2}\right) \tag{40}$$

respectively. The case $v_0 \approx \pi/2$ allows a sharp crack to be described. Eq. (39) can be re-written as:

$$\xi = \mathrm{Arcsinh}\left\{k_2 \cdot \sinh\frac{z}{k_1}\right\} \tag{41}$$

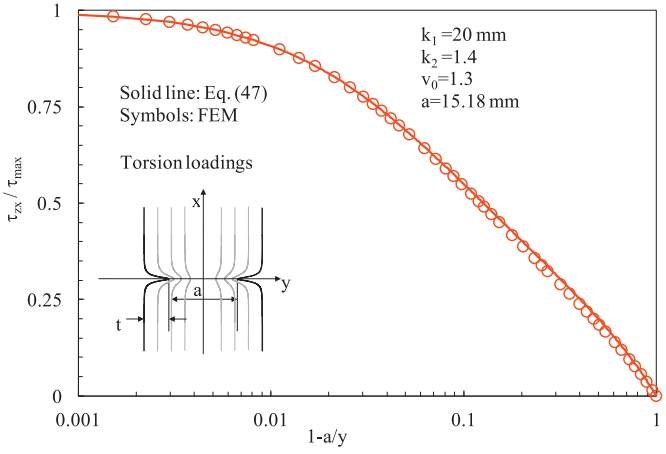

Fig. 9. Plot of the stress component along the notch bisector line. The stress component is normalised with respect to the maximum shear stress. Circumferential hyperbolic notch, as given by Eq. (39), in a finite size axis-symmetric shaft under torsion.

Substituting Eq. (41) into Eq. (15) results in:

$$\tau_{zx} - i\tau_{zy} = \varsigma \frac{d\xi(z)}{dz} = A \frac{k_2 \cdot \mathrm{Cosh}\left[\frac{z}{k_1}\right]}{k_1\sqrt{1 + k_2^2 \cdot \mathrm{Sinh}^2\left[\frac{z}{k_1}\right]}} \tag{42}$$

where A is a real constant to determine. Introducing the following auxiliary variables:

$$z_1 = k_2 \cdot \mathrm{Cosh}\left[\frac{z}{k_1}\right] = r_1 e^{i\theta_1} \quad z_2 = k_1\sqrt{1 + k_2^2 \cdot \mathrm{Sinh}^2\left[\frac{z}{k_1}\right]} = r_2 e^{i\theta_2} \tag{43}$$

stress component can be written as in Eq. (44):

$$\tau_{zx} = A\frac{r_1}{r_2}\cos(\theta_1 - \theta_2) \qquad \tau_{zy} = -A\frac{r_1}{r_2}\sin(\theta_1 - \theta_2) \tag{44}$$

In the case of antiplane shear loadings, along the notch bisector line Eq. (44) simplifies to give:

$$\tau_{zx} = A\frac{k_2 \cos(y/k_1)}{k_1\sqrt{1 - k_2^2 \cdot \sin^2(y/k_1)}} \tag{45}$$

and parameter A can be expressed as a function of the far applied nominal stress, $A = \tau_n \cdot k_1$.

Alternatively, parameter A can also be determined as a function of the maximum tip stress:

$$A = \tau_{max}\frac{k_1\sqrt{1 - k_2^2 \cdot \sin^2(a/k_1)}}{k_2 \cos(a/k_1)} \tag{46}$$

Different from before, in the case of torsion loading of an axis-symmetric notched solid, the stress field along the notch bisector can be approximately written as:

$$\tau_{zx} = \tau_{max}\frac{k_1\sqrt{1 - k_2^2 \cdot \sin^2(a/k_1)}}{k_2 \cos(a/k_1)} \frac{k_2 \cos(y/k_1)}{k_1\sqrt{1 - k_2^2 \cdot \sin^2(y/k_1)}} \times \frac{y}{a} \tag{47}$$

where a is the radius of the net section.

A comparison between the analytical solution given by Eq. (47) and the results from a FE analysis carried out on an axis-symmetric notched shaft under torsion is shown in Fig. 9, where a very satisfactory agreement can be noted.

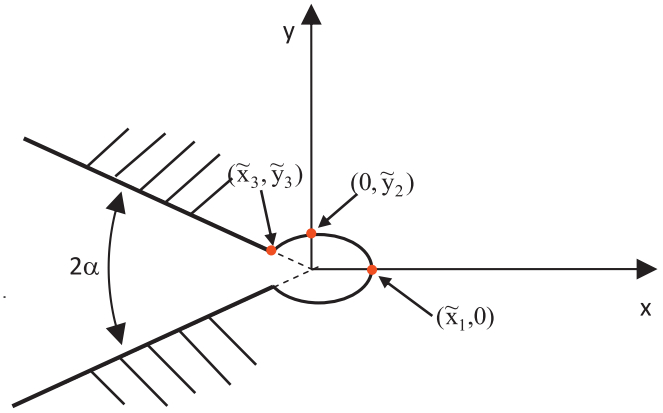

Fig. 10. V-notch with an elliptical rounded tip as given by Eq. (48).

4.5. V-notch with an elliptical rounded tip

Consider the mapping shown in Fig. 10:

$$z = \left\{(1-k)\xi + k\sqrt{4a^{2/q} + \xi^2}\right\}^q \tag{48}$$

where $z = x + iy$, $\xi = u_0 + iv$, k and a are two constants. Such a mapping allows the case of a V notch with an elliptical rounded tip to be described by the case $u_0 = 0$. Parameter q is linked to the notch opening angle by the expression $q = \frac{2\pi - 2\alpha}{\pi}$.

The following three relevant sites can be deduced based on the transformation given by Eq. (48):

1. Intersection of the ellipse with the x-axis (notch tip), given by the condition $v = 0$ and resulting in:

$$\tilde{x}_1 = (2k)^q \cdot a \tag{49}$$

2. Intersection of the ellipse with the y-axis, given by

$$\tilde{v}_2 = 2ka^{1/q} \times \mathrm{Tan}\frac{\pi}{2q} \times \left\{\frac{(1-k)^2}{\mathrm{Tan}^2\frac{\pi}{2q}} + k^2\right\}^{-0.5} \tag{50}$$

The associated value of y is:

$$\tilde{y}_2 = \left\{(1-k)^2\tilde{v}_1^2 + k^2\left(4a^{2/q} - \tilde{v}_1^2\right)\right\}^{q/2} \tag{51}$$

3. The intersections between the rectilinear flanks and the ellipse. Those points are characterised by the value $\tilde{v}_3 = \pm 2a^{1/q}$ and the associated Cartesian coordinates are:

$$\tilde{x}_3 = \{(1-k)\tilde{v}_2\}^q \cos\frac{\pi}{2}q \qquad \tilde{y}_3 = \{(1-k)\,\tilde{v}_2\}^q \sin\frac{\pi}{2}q \tag{52}$$

Eq. (48) can be re-written as:

$$\xi = \frac{(k-1)\cdot z^{1/q} + k\cdot\sqrt{z^{2/q} - 4a^{2/q}(2k-1)}}{2k-1} \tag{53}$$

Substituting Eq. (53) into Eq. (12) gives:

$$\tau_{zy} + i\tau_{zx} = A\left\{\frac{k-1}{2k-1}\cdot z^{1/q-1} + \frac{k}{2k-1}\frac{z^{2/q-1}}{\sqrt{z^{2/q} - 4a^{2/q}(2k-1)}}\right\} \tag{54}$$

where A is a constant to determine.

Defining the following auxiliary variables:

$$z_1 = z^{2/q} - 8a^{2/q}\left(k - \frac{1}{2}\right) = r_1 e^{i\theta_1} \tag{55}$$

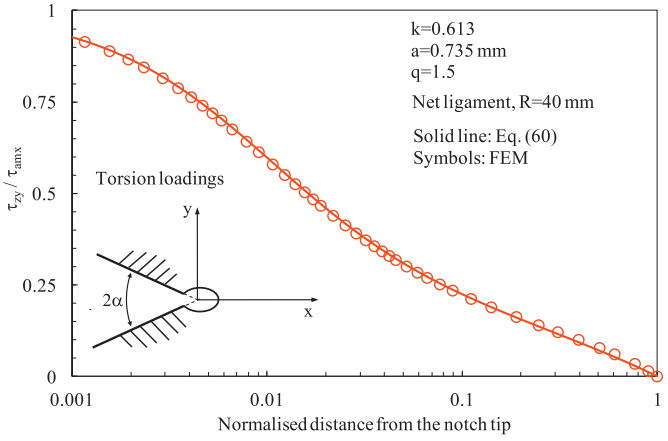

Fig. 11. Plot of the stress component along the notch bisector line. The stress component is normalised with respect to the maximum shear stress. Circumferential V-notch with an elliptical rounded tip in a finite size axis-symmetric shaft under torsion.

stresses can be written as:

$$\begin{aligned}\tau_{zy} &= A\left\{(k-1)\cdot r^{1/q-1}\cos(1/q-1)\theta \right.\\ &\left. \quad + k\cdot\frac{r^{2/q-1}}{r_1^{1/2}}\cos\left[(2/q-1)\theta-\frac{\theta_1}{2}\right]\right\}\\ \tau_{zx} &= A\left\{(k-1)\cdot r^{1/q-1}\sin(1/q-1)\theta \right.\\ &\left. \quad + k\cdot\frac{r^{2/q-1}}{r_1^{1/2}}\sin\left[(2/q-1)\theta-\frac{\theta_1}{2}\right]\right\}\end{aligned} \tag{56}$$

Parameter A can be written as a function of the maximum notch tip stress (for $r=\tilde{x}_1$):

$$A=\frac{\tau_{max}}{\left\{(k-1)\cdot\tilde{x}_1^{1/q-1}+k\cdot\frac{\tilde{x}_1^{2/q-1}}{\tilde{r}_1^{1/2}}\right\}}=\frac{\tau_{max}}{\omega} \tag{57}$$

where:

$$\tilde{r}_1=\tilde{x}_1^{2/q}-8a^{2/q}\left(k-\frac{1}{2}\right) \tag{58}$$

Along the notch bisector line the stress field simplifies to give:

$$\tau_{zy}=\frac{\tau_{max}}{\omega}\left\{(1-k)\cdot r^{1/q-1}+k\cdot\frac{r^{2/q-1}}{r_1^{1/2}}\right\} \tag{59}$$

In the case of an axis-symmetric notched shaft under torsion loadings, Eq. (59) becomes:

$$\tau_{zy}=\frac{\tau_{max}}{\omega}\left\{(1-k)\cdot r^{1/q-1}+k\cdot\frac{r^{2/q-1}}{r_1^{1/2}}\right\}\times\left(1-\frac{r-\tilde{x}_1}{R}\right) \tag{60}$$

where R is the radius of the net section.

A comparison between the analytical solution given by Eq. (60) and the results from a FE analysis carried out on an axis-symmetric notched shaft under torsion is shown in Fig. 11, where a very satisfactory agreement can be noted.

5. Schwarz-Christoffel transformation for description of finite notches in infinite plates

5.1. Introductory remarks

In Section 2 a logical approach to define the stress complex potential was proposed according to which, once the conformal map is defined, the complex potential is determined, as well. This makes some methodologies such as Schwarz-Christoffel transformation very attractive to determine analytical solutions for the stress fields caused by sharp notches. Indeed, this transformation allows describing any polygonal domain automatically, thus simplifying the construction of suitable complex potentials for various notches.

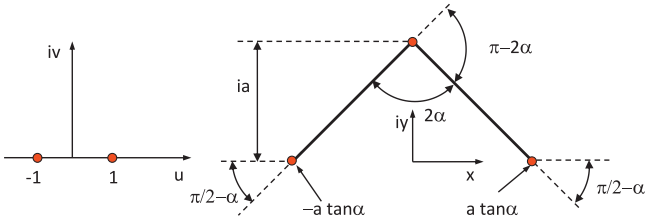

Fig. 12. Finite V-notch with general depth a and opening 2α.

In general terms, the Schwarz-Christoffel Mapping (SCM) function can be written as (Driscoll and Trefethen, 2002).

$$z=f(\xi)=C\int^{\xi}\prod_{j=1}^{n}\frac{dw}{(w-a_j)^{1-\frac{\alpha_j}{\pi}}} \tag{61}$$

where C is a constant. Such a general function maps the real axis to the edges of a polygon with n sides and interior angles α_j, whereas a_j represents the vertices of the polygon in the complex plane.

According to the SCM, the domain boundary is described by $v(x, y)=0$ so, from now on, Eq. (15) will be referenced to define the stress complex potential.

5.2. The shallow V-notch

Let us consider the case of a finite sharp V-notch in an infinite solid subjected to a remote shear stress $\tau_{zx}=\tau_\infty$ (Fig. 12). Thanks to the SCM the conformal map describing the notch profile and the corresponding first derivative are:

$$Z'(\xi)=A\frac{\xi^{1-2\alpha/\pi}}{\left(\xi^2-1\right)^{1/2-\alpha/\pi}}\qquad Z(\xi)=B+\int^{\xi}Z'(w)dw \tag{62}$$

where A and B are complex constants. However, since the stress field is linked to $Z'(\xi)$, constant A suffices to be determined, taking advantage of the following boundary conditions:

$$\begin{cases}Z(\xi=0)=ia\\ Z(\xi=1)=a\tan\alpha\end{cases} \tag{63}$$

which give:

$$A=\frac{a\sqrt{\pi}}{\cos\alpha\,\Gamma\left(1-\frac{\alpha}{\pi}\right)\Gamma\left(\frac{1}{2}+\frac{\alpha}{\pi}\right)} \tag{64}$$

where $\Gamma(t)=\int_0^\infty x^{t-1}\cdot e^{-x}dx$ is the gamma function. Substituting Eq. (62) into Eq. (15):

$$\tau_{zx}-i\tau_{zy}=\varsigma\frac{d\xi(z)}{dz}=\varsigma\left(\frac{dZ(\xi)}{d\xi}\right)^{-1}=\tau_\infty\frac{\left(\xi^2-1\right)^{1/2-\alpha/\pi}}{\xi^{1-2\alpha/\pi}} \tag{65}$$

where $\tau_\infty=\lim_{|\xi|\to\infty}\tau_{zx}-i\tau_{zy}$ is the far applied shear stress. Accordingly, the explicit knowledge of stress components requires the function $\xi=\xi(Z)$ to be known and, in general, this is far from easy.

However, if the stresses near the notch tip are of interest, the process can be considerably simplified. To this end, one should note that, thanks to *De L' Hospital*'s rule, the following equations are valid:

$$\lim_{\xi\to0}\frac{Z-ia}{\xi^{1-2\alpha/\pi}}\overset{H}{=}\lim_{\xi\to0}\frac{A}{1-2\alpha/\pi}\frac{\xi}{\left(\xi^2-1\right)^{1/2-\alpha/\pi}}=0 \tag{66}$$

$$\lim_{\xi\to 0}\left[(1-2\alpha/\pi)\frac{Z-ia}{\xi^{2-2\alpha/\pi}}\right]\xi=\lim_{\xi\to 0}\left[\frac{1-2\alpha/\pi}{2(1-\alpha/\pi)}\frac{Z'(\xi)}{\xi^{1-2\alpha/\pi}}\right]\xi \tag{67}$$

So that invoking a Taylor series expansion near $\xi=0$:

$$\frac{Z-ia}{\xi^{1-2\alpha/\pi}}=\lim_{\xi\to 0}\left[\frac{Z'(\xi)}{\xi^{1-2\alpha/\pi}}-\frac{1-2\alpha/\pi}{2(1-\alpha/\pi)}\frac{Z'(\xi)}{\xi^{1-2\alpha/\pi}}\right]\xi+\vartheta\left(\xi^2\right) \tag{68}$$

Now, introducing the change of variables $z=Z\text{-}ia$ and rearranging, Eq. (68) gives:

$$z\approx\frac{A}{2\exp\left[(\pi/2-\alpha)i\right](1-\alpha/\pi)}\xi^{2(1-\alpha/\pi)} \tag{69}$$

or, equivalently:

$$\xi\approx e^{\left[(\pi/2-\alpha)/2(1-\alpha/\pi)i\right]}\left[\frac{2(1-\alpha/\pi)}{A}\right]^{1/2(1-\alpha/\pi)}z^{1/2(1-\alpha/\pi)} \tag{70}$$

Eventually, substituting Eq. (70) into Eq. (65) gives:

$$\tau_{zx}-i\tau_{zy}=\tau_\infty e^{\frac{\pi}{2}\frac{q-1}{q}i}\left[\frac{A}{q}\right]^{1/q-1}z^{1/q-1} \tag{71}$$

where the equality $2\alpha=\pi(2\text{-}q)$ has been used. The Notch Stress Intensity Factor for this geometry can be easily determined by the definition $K_3=\sqrt{2\pi}\lim_{y\to 0}\tau_{zx}y^{1-1/q}$, which gives:

$$\begin{aligned}K_3&=\tau_\infty\sqrt{2\pi}\left[\frac{A}{q}\right]^{1/q-1}\\&=\tau_\infty\sqrt{2\pi}\left[\frac{a\sqrt{\pi}}{q\cos\alpha\,\Gamma\left(1-\frac{\alpha}{\pi}\right)\Gamma\left(\frac{1}{2}+\frac{\alpha}{\pi}\right)}\right]^{1-1/q}\\&=\tau_\infty\cdot k_3\cdot a^{1-1/q}\end{aligned} \tag{72}$$

where:

$$k_3=\sqrt{2\pi}\left[\frac{\sqrt{\pi}}{q\cos\alpha\,\Gamma\left(1-\frac{\alpha}{\pi}\right)\Gamma\left(\frac{1}{2}+\frac{\alpha}{\pi}\right)}\right]^{1-1/q} \tag{73}$$

Being the solid infinite, Eq. (72) is valid both for a prismatic body under longitudinal shear and for an axisymmetric shaft weakened by a circumferential pointed V notch.

Recently Zappalorto et al. (2009) provided an approximate expression for parameter k_3, based on a best fitting of the results from numerical analyses carried out on torque loaded circumferential bodied with shallow notches ($0°\le 2\alpha\le 150°$). Such an expression reads as:

$$k_{3s}=\sqrt{\pi}\left(-\frac{3779}{878}\cdot s_3^2-\frac{90}{119}\cdot s_3+\frac{527}{312}\right) \tag{74}$$

where $s_3=(\alpha-\pi/2)/(\pi-\alpha)$.

Fig. 13 shows a comparison between Eq. (73) and Eq. (74), both of them being also compared to numerical results. The accuracy of Eq. (73) is noteworthy.

5.3. The finite inclined crack in an infinite medium

Consider the case of a finite length inclined crack in an infinite medium subjected to a remote shear stress (Fig. 14). The corresponding bending problem was analysed by Hasebe and Inohara (1980) and later extended to the quasi-orthotropic case by Hasebe and Sato (2013).

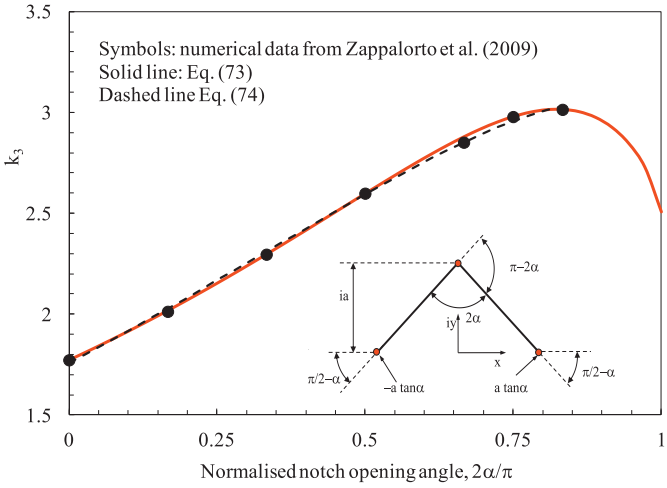

Fig. 13. Comparison between Eqs. (73), (74) and numerical data from Zappalorto et al. (2009). Shallow V-notch under torsion.

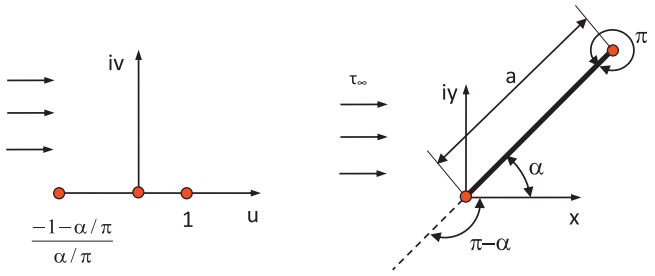

Fig. 14. Finite length inclined crack in an infinite medium subjected to a remote shear stress.

According to SCM, the first derivative of the mapping can be expressed as:

$$Z'(\xi)=a\left(\frac{\alpha}{\pi-\alpha}\right)^{1-\frac{\alpha}{\pi}}\frac{\xi}{(\xi-1)^{1-\alpha/\pi}\left(\xi-\frac{\alpha-\pi}{\alpha}\right)^{\alpha/\pi}} \tag{75}$$

Accordingly:

$$Z(\xi)=a\left(\frac{\alpha}{\pi-\alpha}\right)^{1-\frac{\alpha}{\pi}}(\xi-1)^{\alpha/\pi}\left(1+\frac{\alpha/\pi\,\xi}{1-\alpha/\pi}\right)^{1-\alpha/\pi} \tag{76}$$

Taking advantage of Eq. (15):

$$\tau_{zx}-i\tau_{zy}=\tau_\infty\frac{(\xi-1)^{1-\alpha/\pi}\left(\xi+\frac{1-\alpha/\pi}{\alpha/\pi}\right)^{\alpha/\pi}}{\xi} \tag{77}$$

where $\tau_\infty=\lim_{|\xi|\to\infty}\tau_{zx}-i\tau_{zy}$ is the far applied shear stress.

Consider now the following MacLaurin series expansion:

$$\begin{aligned}\frac{Z-ae^{i\alpha}}{\xi}&=\lim_{\xi\to 0}\left[\frac{Z'(\xi)}{\xi}-\frac{Z-ae^{i\alpha}}{\xi^2}\right]\xi\\&\quad+\vartheta\left(\xi^2\right)\overset{H}{=}\lim_{\xi\to 0}\left[\frac{Z'(\xi)}{\xi}-\frac{1}{2}\frac{Z'(\xi)}{\xi}\right]\xi+\vartheta\left(\xi^2\right)\end{aligned} \tag{78}$$

where the latter substitution is guaranteed by *De L'Hospital*'s rule. Accordingly:

$$\frac{Z-ae^{i\alpha}}{\xi}\approx\frac{1}{2}\frac{a}{e^{i(\pi-\alpha)}}\left(\frac{\alpha}{\pi-\alpha}\right)\xi \tag{79}$$

Then, introducing the change of variables $z=Z\text{-}ae^{i\alpha}$:

$$z\approx\frac{1}{2}\frac{a}{e^{i(\pi-\alpha)}}\left(\frac{\alpha}{\pi-\alpha}\right)\xi^2 \tag{80}$$

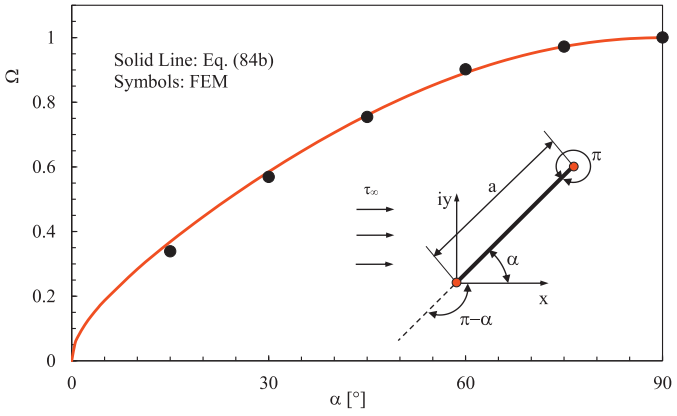

Fig. 15. Comparison between Eq. (84b) and the results from FE analyses. Inclined crack in a solid under antiplane shear. (The FE analysis was conducted using the following dimensions: width, $W = 240$ mm, height, $H = 240$ mm and length of the edge crack, $a = 10$ mm).

or equivalently:

$$\xi \approx \sqrt{2} e^{i(\pi-\alpha)/2} \left(\frac{\pi-\alpha}{\alpha}\right)^{\frac{1}{2}} \left(\frac{z}{a}\right)^{\frac{1}{2}} \tag{81}$$

and, substituting Eq. (81) into Eq. (77) gives:

$$\tau_{zx} - i\tau_{zy} = \tau_\infty \frac{\sqrt{2}}{2} e^{i(\pi-\alpha)/2} \left(\frac{\pi-\alpha}{\alpha}\right)^{\frac{\alpha}{\pi}-\frac{1}{2}} \left(\frac{a}{z}\right)^{\frac{1}{2}} \tag{82}$$

or, in polar stress components:

$$\tau_{zr} - i\tau_{z\theta} = e^{i\theta}(\tau_{zx} - i\tau_{zy}) = \tau_\infty \frac{\sqrt{2}}{2} e^{i(\pi-\alpha)/2+\theta/2} \left(\frac{\pi-\alpha}{\alpha}\right)^{\frac{\alpha}{\pi}-\frac{1}{2}} \left(\frac{a}{r}\right)^{\frac{1}{2}} \tag{83}$$

Noting that along the crack plane $\theta = \alpha$, the stress intensity factor turns out to be:

$$K_{III} = \sqrt{2\pi} \lim_{y\to 0} \tau_{zx} r^{1/2} = \tau_\infty \sqrt{\pi a} \left(\frac{\pi-\alpha}{\alpha}\right)^{\frac{\alpha}{\pi}-\frac{1}{2}} = \Omega \cdot \tau_\infty \sqrt{\pi a} \tag{84a}$$

where:

$$\Omega = \left(\frac{\pi-\alpha}{\alpha}\right)^{\frac{\alpha}{\pi}-\frac{1}{2}} \tag{84b}$$

A comparison between the analytical solution given by Eq. (84b) and the results from FE analyses carried out on rectangular plates weakened by shallow inclined cracks is shown in Fig. 15, where an excellent agreement can be noted.

5.4. Rectangular cut out under longitudinal shear

Consider a rectangular cutout under longitudinal shear (Fig. 16). The conformal mapping to be used to describe the notch profile can be chosen as:

$$Z(\xi) = D\, E_2\left[\xi, \frac{b}{a}\right] / E_{2c}\left[\frac{b}{a}\right] \tag{85}$$

where E_2 is the elliptic integral of the second kind, $E_2(x, y) = \int_0^x \sqrt{1 - y^2 \sin^2\theta}\, d\theta$, whereas $E_{2c}(y)$ is the complete elliptical integral of the second kind. Under the condition b<a, the height of the cutout, h, can be expressed as:

$$h = \mathrm{Im}\left\{ \lim_{\nu\to\infty} D \cdot E_2[\pi/2 + i\nu, b/a] / E_{2c}[b/a] \right\} \tag{86}$$

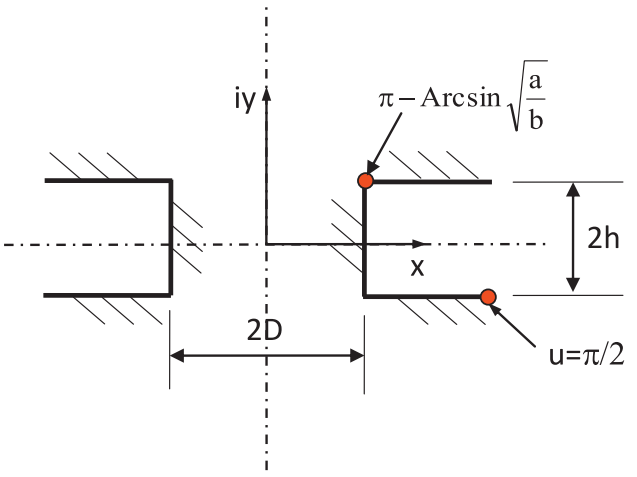

Fig. 16. Schematic of a body weakened by a rectangular cutout.

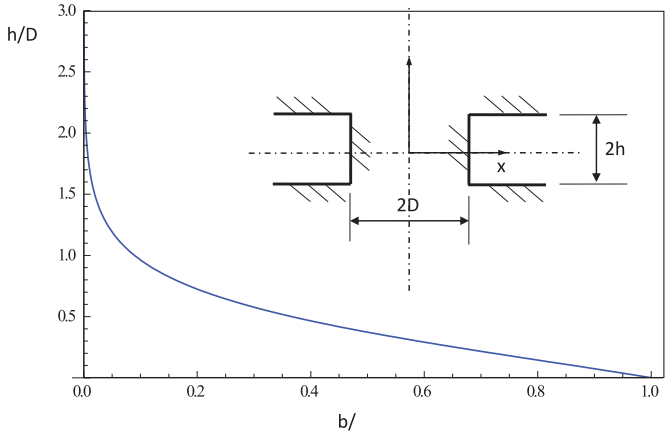

Fig. 17. Plot of Eq. (87).

Accordingly, assuming a and b to be integers, the ratio h/D can be written as:

$$\frac{h}{D} = -2\sqrt{\frac{b}{a}} \frac{\left\{\cdot E_{2c}\left[1-\frac{a}{b}\right] - \frac{a}{b}\cdot E_{1c}\left[1-\frac{a}{b}\right]\right\} - \mathrm{Im}\left\{\left[E_{2c}\left[\frac{a}{b}\right] - \left(1-\frac{a}{b}\right)E_{1c}\left[\frac{a}{b}\right]\right]\right\}}{E_{2c}\left[\frac{b}{a}\right]} \tag{87}$$

where $E_{1c}(y) = \int_0^{\pi/2} \frac{d\theta}{\sqrt{1-y^2\sin^2\theta}}$ is the complete elliptic integral of the first kind. Eq. (87) is plotted in Fig. 16.

Invoking Eq. (12) together with Eq. (87), stresses can be written as:

$$\tau_{zy} + i\tau_{zx} = \varsigma \frac{d\xi(z)}{dz} = \varsigma \left(\frac{dZ(\xi)}{d\xi}\right)^{-1} = \frac{\varsigma}{D} \frac{E_{2c}[b/a]}{\sqrt{1 - b/a \sin^2\xi}} \tag{88}$$

To define stresses in Cartesian coordinates near one of the vertices we need to find $\xi = \xi(Z)$. To this end, consider the Taylor expansion near $\psi = \pi - \arcsin\sqrt{a/b}$:

$$\begin{aligned} \frac{Z - (D + ih)}{\sqrt{1 - b/a\sin^2\xi}} &= 0 + \lim_{\xi\to\psi} \left[\frac{Z'(\xi)}{\sqrt{1 - b/a\sin^2\xi}} - \frac{1}{2} \frac{Z(\xi) - (D+ih)}{\left(1 - b/a\sin^2\xi\right)^{3/2}} \right. \\ &\quad \left. \times \left(-2\frac{b}{a}\sin\xi\cos\xi\right) \right] (\xi - \psi) + \vartheta(\xi - \psi)^2 \\ &\approx \lim_{\xi\to\psi} \left[\frac{2}{3} \frac{Z'(\xi)}{\sqrt{1 - b/a\sin^2\xi}} \right] (\xi - \psi) \\ &= \frac{2}{3} \frac{D}{E_{2c}[b/a]} (\xi - \psi) \end{aligned} \tag{89}$$

Introducing the change of coordinates $z = Z\text{-}(D + ih)$:

$$z \approx \frac{2}{3}\sqrt{1 - b/a\sin^2\xi}\,\frac{D}{E_{2c}[b/a]}(\xi - \psi) \tag{90}$$

and recalling that:

$$\begin{aligned} 1 - b/a\sin^2\xi &\approx -2b/a\,\sin\xi\cos\xi\,(\xi - \psi) \\ &= -2b/a\sqrt{a/b}\sqrt{1 - a/b}(\xi - \psi) \end{aligned} \tag{91}$$

one obtains:

$$\xi \approx \psi + \frac{z^{2/3}e^{-i\pi/2}}{\left(\frac{2}{3}\sqrt{2b/a\sqrt{a/b}\sqrt{a/b - 1}}\frac{D}{E_{2c}[b/a]}\right)^{\frac{2}{3}}} \tag{92}$$

Moreover, noting that:

$$\sqrt{-2b/a\sqrt{a/b}\sqrt{1 - a/b}} = \sqrt{2b/a\sqrt{a/b}\sqrt{a/b - 1}}e^{i3/4\pi} \tag{93}$$

substituting into Eq. (88) and rearranging:

$$\tau_{zy} + i\tau_{zx} = \frac{\zeta}{D}\frac{(E_{2c}[b/a])^{2/3}}{\left(2b/a\sqrt{a/b}\sqrt{a/b - 1}\right)^{1/3}}e^{-i\pi/2}\left(\frac{2}{3}\right)^{1/3}\left(\frac{D}{z}\right)^{1/3} \tag{94}$$

Moving to polar coordinates:

$$\begin{aligned} \tau_{z\theta} + i\tau_{zr} &= e^{i\theta}(\tau_{zy} + i\tau_{zx}) \\ &= \frac{\zeta}{D}\frac{(E_{2c}[b/a])^{2/3}}{\left(2b/a\sqrt{a/b}\sqrt{a/b - 1}\right)^{1/3}}e^{-i\pi/2 + 3/4\theta}\left(\frac{2}{3}\right)^{1/3}\left(\frac{D}{r}\right)^{1/3} \end{aligned} \tag{95}$$

Taking advantage of Eq. (95) it is trivial to determine an analytical solution for the Notch Stress Intensity Factor at the corner of the cut-out, K_3:

$$K_3 = \sqrt{2\pi}\lim_{r\to 0,\theta = 3/4\pi}\tau_{z\theta}\cdot r^{1/3} = \sqrt{2\pi}\frac{\zeta}{D^{2/3}}\frac{(E_{2c}[b/a])^{2/3}}{\left(2\sqrt{1 - b/a}\right)^{1/3}}\left(\frac{2}{3}\right)^{1/3} \tag{96}$$

Consider now a prismatic solid of unit thickness, invoking the equilibrium of shear forces, the following equation holds valid:

$$T_{tot} = 2\int_0^D \zeta\frac{d\xi(Z)}{dZ}dZ = 2\int_0^{\pi/2}\zeta\,d\xi = \pi\zeta \tag{97}$$

where T_{tot} is the applied shear force. Accordingly,

$$\zeta = \frac{T_{tot}}{\pi} \tag{98}$$

Substituting Eq. (98) into Eq. (96) and rearranging results in the following expression for the mode III NSIF:

$$K_3 = \tau_{nn}\cdot\left\{\left(\frac{2}{3}\right)^{1/3}2\sqrt{\frac{2}{\pi}}\frac{(E_{2c}[b/a])^{2/3}}{\left(2\sqrt{1 - b/a}\right)^{1/3}}\right\}\cdot D^{1/3} = \tau_{nn}\cdot k_{3R}\cdot D^{1/3} \tag{99}$$

where $\tau_{nn} = \frac{T_{tot}}{2D}$ is the nominal shear stress and:

$$k_{3R} = \left(\frac{2}{3}\right)^{1/3}2\sqrt{\frac{2}{\pi}}\frac{(E_{2c}[b/a])^{2/3}}{\left(2\sqrt{1 - b/a}\right)^{1/3}} \tag{100}$$

A comparison between Eq. (100) and the results from FEA is shown in Fig. 18, where a very satisfactory agreement can be noted.

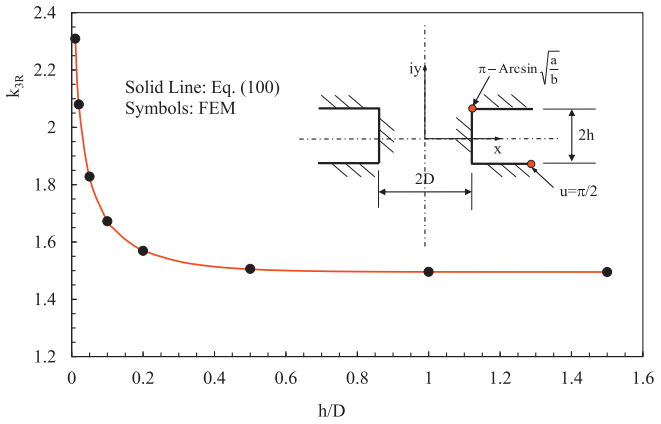

Fig. 18. Comparison between Eq. (100) and the results from FE analyses. Rectangular cutout in a prismatic solid under antiplane shear. (The FE analysis was conducted using the following dimensions: width, $W = 240$ mm, height, $H = 240$ mm and notch depth, $a = 100$ mm).

6. Conclusions

Mode III is a common loading scenario in several engineering applications, from e.g. power transmission shafts to fastened joints. This contribution proposes a general approach to solve, in closed form, the stress and strain fields in cracked or notched bodies subjected to *anti-plane shear* or *torsional* loadings. Based on the analyses and the discussions presented in this study, the following conclusions can be formulated:

1. the mode III stress fields can be uniquely determined by the introduction of a complex potential. Provided the domain of the problem can be described by an analytic function and the zero-stress condition is applied on a straight line in the transformed domain, *the mentioned complex potential is proportional to the first derivative of the mapping*;
2. there is no need to make arbitrary assumptions on the stress complex potential. *Once the geometry of the problem is defined, the potential is uniquely determined.* Accordingly, the problem is not guessing the right potential but finding the correct conformal mapping of the problem;
3. when the Schwarz-Christoffel approach is adopted, the solution can be found by simple geometrical construction. This is similar in spirit to the Mohr's circles approach for the determination of principal stresses;
4. the foregoing considerations make the solution of even complex geometries rather simple as the analyses presented in the manuscript clearly show. Several completely new solutions such as the rectangular cut, finite V-notch, elliptic keyhole have been presented in this work leveraging on the proposed approach.
5. finally, another application of the proposed methodology is the calculation of the three-dimensional stress field in notched plates with finite thickness. In such a case, as shown in (Lazzarin et al., 2012, 2015 and Zappalorto and Lazzarin 2013), the stress field is governed by two uncoupled equations in the two-dimensional space. The solution of the first equation requires the same methodologies corresponding to plane notch problems. The second equation corresponds to the related out-of-plane shear notch problem and it can be solved by means of the formulation proposed in the present work.

Acknowledgments

Marco Salviato acknowledges the financial support by the William E. Boeing Department of Aeronautics and Astronautics as well as the College of Engineering at the University of Washington through the start-up package.

Michele Zappalorto acknowledges the financial support by the University of Padova within the project CPDA145509 "*Advanced theoretical and experimental analysis of damage initiation and evolution in polymer nanocomposites*".

References

Cheng, C.Z., Ge, S.Y., Yao, S.L., Niu, Z.R., Recho, N., 2016. Singularity analysis for a V-notch with angularly inhomogeneous elastic properties. Int. J. Solids Struct. 78–79, 138–148.

Creager, M., Paris, P.C., 1967. Elastic field equations for blunt cracks with reference to stress corrosion cracking. Int. J. Fract. Mech. 3, 247–252.

Driscoll, T.A., Trefethen, L.N., 2002. Schwarz-Christoffel mapping. Cambridge Monographs on Applied and Computational Mathematics 8. Cambridge University Press.

Dunn, M.L., Suwito, W., Cunningham, S., 1997. Stress intensities at notch singularities. Eng. Fract. Mech. 57, 417–430.

Filon, L.N.G., 1900. On the resistance to torsion of certain forms of shafting with special reference to the effect of keyways. Philos. Trans. R. Soc. A 193, 309–352.

Greenberg, M.D., 2001. Advanced Engineering Mathematics. Prentice Hall, New Jersey.

Hamada, M., Kitagawa, H., 1968. Numerical solutions of two-dimensional elastic plastic problems by conformal mapping and finite difference method (elastic torsion of circumferentially grooved shafts). Bull. Japan Soc. Mech. Eng. 11, 605–611.

Hasebe, N., Inohara, S., 1980. Stress analysis of a semi-infinite plate with an oblique edge crack. Ing. Arch. 49, 51–62.

Hasebe, N., Sato, M., 2013. Stress analysis of quasi-orthotropic elastic plane. Int. J. Solids Struct. 50, 209–216.

Kazberuk, A., Savruk, M.P., Chornenkyi, A.B., 2016. Stress distribution at sharp and rounded V-notches in quasi-orthotropic plane. Int. J. Solids Struct. 85–86, 134–143.

Kullmer, G., 1992. Elastic stress fields in the vicinity of a narrow notch with circular root. In: Reliability and Structural Integrity of Advanced Materials. Proceedings of the 9th Biennial European Conference on Fracture (ECF 9), Vol. II. Varna, Bulgaria, pp. 905–910.

Lazzarin, P., Zappalorto, M, 2012. A three-dimensional stress field solution for pointed and sharply radiused V-notches in plates of finite thickness. Fatigue Fract. Eng. M Struct. 35, 1105–1119.

Lazzarin, P., Zappalorto, M., Berto, F., 2015. Three-dimensional stress fields due to notches in plates under linear elastic and elastic-plastic conditions. Fatigue Fract. Eng. M 38, 140–153.

Lazzarin, P., Zappalorto, M., Yates, J.R., 2007. Analytical study of stress distributions due to semi-elliptic notches in shafts under torsion loading. Int. J. Eng. Sci. 45, 308–328.

Matthews, G.J., Hoke, C.J., 1971. Solution of axis-symmetric torsion problems by point matching. J. Strain. Anal. 6, 124–133.

Neuber, H., 1958. Theory of Notch Stresses: Principles for Exact Calculation of Strength with Reference to Structural Form and Material. Splinger-Verlag, Berlin.

Neuber, H., 1985. Kerbspannungslehre: Theorie Der Spannungskonzetration; Genaue Berechnung Der Festigkeit. Splinger-Verlag, Berlin.

Noda, N., Takase, Y., 2006. Stress concentration formula useful for all notch shape in a round bar (comparison between torsion, tension and bending). Int. J. Fatigue 28, 151–163.

Peterson, R.E., 1974. Stress Concentration Factors. John Wiley & Sons, New York.

Qian, J., Hasebe, N., 1997. Property of Eigenvalues and eigenfunctions for an interface V-notch in antiplane elasticity. Eng. Fract. Mech. 56, 729–734.

Rushton, K.R., 1967. Stress concentrations arising in the torsion of grooved shafts. Int. J. Mech. Sci. 9, 697–705.

Savin, G.N., 1970. Stress Distribution Around Holes. NASA, Washington.

Savruk, M.P., Kazberuk, A., Tarasiuk, G., 2012. Distribution of stresses over the contour of rounded V-shaped notch under antiplane deformation. Mater. Sci. 47, 717–725.

Seweryn, A., Molski, K., 1996. Elastic stress singularities and corresponding generalized stress intensity factors for angular corners under various boundary condition. Eng. Fract. Mech. 55, 529–556.

Shepherd, W.M., 1932. The torsion and flexure of shafting with keyways or cracks. Proc. Roy. Soc. Lond. 138, 607–634.

Sokolnikoff, I.S., 1983. Mathematical Theory of Elasticity. Krieger Pub Co.

Timoshenko, S.P., Goodier, J.N., 1970. Theory of Elasticity, 3rd Edition McGraw-Hill, New York.

Wigglesworth, L.A., 1939. Flexure and torsion of an internally cracked shaft. Proc. Roy. Soc. Lond. 170, 365–391.

Wigglesworth, L.A., Stevenson, A.C., 1939. Flexure and torsion of cylinders with cross-sections bounded by orthogonal circular arcs. Proc. Roy. Soc. Lond. A184, 391–414.

Zappalorto, M., Berto, F., Lazzarin, P., 2011. Practical expressions for the notch stress concentration factors of round bars under torsion. Int. J. Fatigue 33, 382–395.

Zappalorto, M., Carraro, P.A., 2015. Stress distributions for blunt cracks and radiused slits in anisotropic plates under in-plane loadings. Int. J. Solids Struct. 56-57, 136–141.

Zappalorto, M., Lazzarin, P., 2011a. In-plane and out-of-plane stress field solutions for V-notches with end holes. Int. J. Fract. 168, 167–180.

Zappalorto, M., Lazzarin, P., 2011b. Stress fields due to inclined notches and shoulder fillets in shafts under torsion. J. Strain Anal. Eng. 46, 187–199.

Zappalorto, M., Lazzarin, P., 2012. Torsional stress distributions in tubes with external and internal notches. J. Strain Anal. Eng. 47, 331–340.

Zappalorto, M., Lazzarin, P., 2013. Three-dimensional elastic stress fields ahead of notches in thick plates under various loading conditions. Eng. Fract. Mech. 108, 75–88.

Zappalorto, M., Lazzarin, P., Berto, F., 2009. Elastic notch stress intensity factors for sharply V-notched rounded bars under torsion. Eng. Fract. Mech. 76 (3), 439–453.

Zappalorto, M., Lazzarin, P., Filippi, S., 2010. Stress field equations for U and blunt V-shaped notches in axisymmetric shafts under torsion. Int. J. Fract. 164, 253–269.

Zappalorto, M., Lazzarin, P., Yates, J.R., 2008. Elastic stress distributions resulting from hyperbolic and parabolic notches in round shafts under torsion and uniform antiplane shear loadings. Int. J. Solids Struct. 45, 4879–4901.